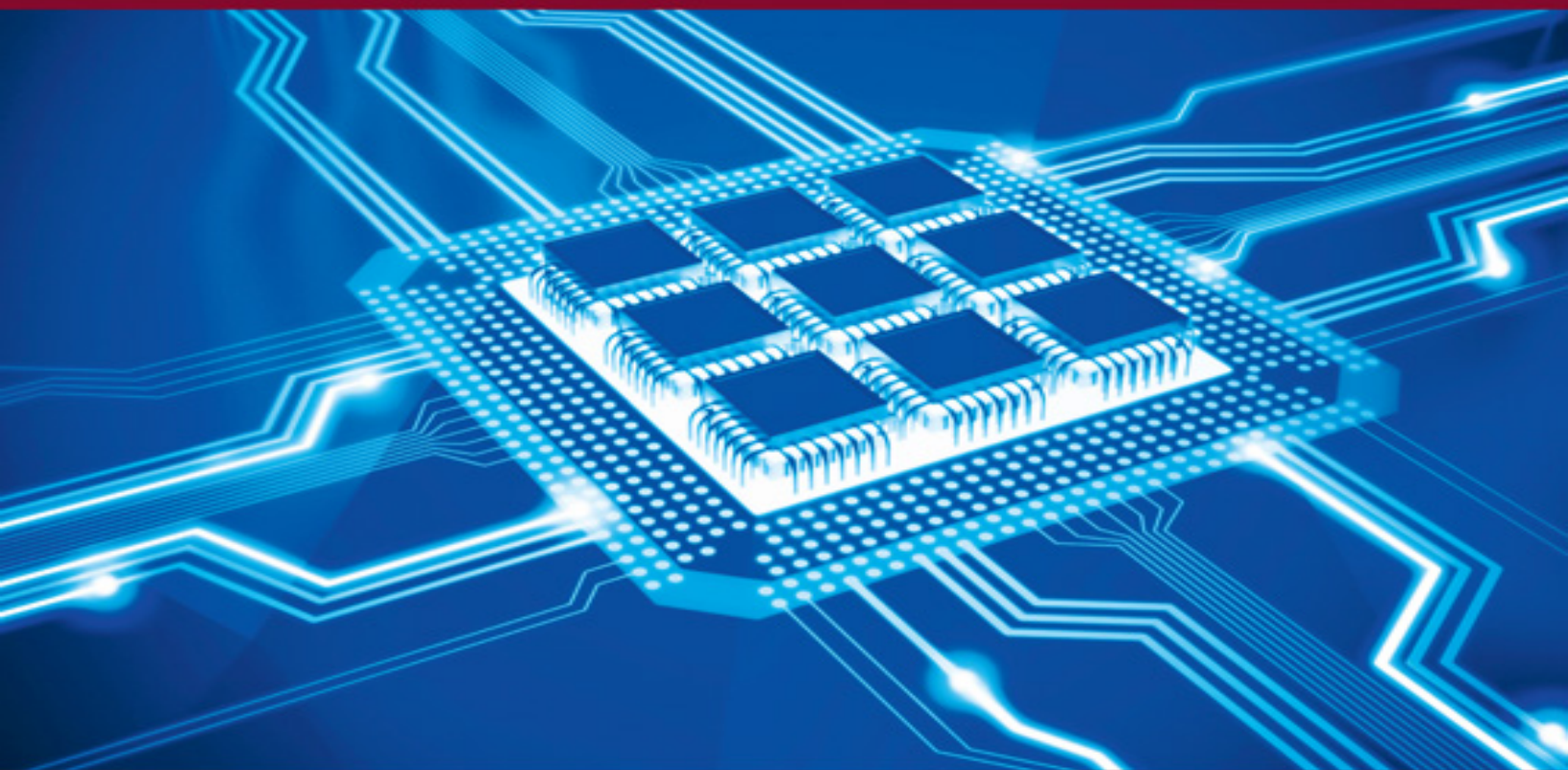


ENERGY SERIES

Smart Power Integration

Mohamed Abouelatta
Ahmed Shaker
Christian Gontrand



ISTE

WILEY

Table of Contents

[Cover](#)

[Title Page](#)

[Copyright](#)

[Preface](#)

[1 Overview of Smart Power Integration](#)

[1.1. Introduction](#)

[1.2. Smart PIC applications](#)

[1.3. Historical view of the MOS power devices](#)

[1.4. Smart PIC fabrication processes](#)

[1.5. Insulation techniques](#)

[1.6. Motivation of the book](#)

[2 Modular or Hybrid Integration](#)

[2.1. Introduction](#)

[2.2. IGBT technology evolution](#)

[2.3. Assembly technology](#)

[2.4. Thermal aspect](#)

[2.5. Applications fields](#)

[3 Monolithic Integration](#)

[3.1. Functional integration and smart power](#)

[3.2. Transition from low-voltage technology \(CMOS\) to high voltage](#)

[3.3. Combining analog and digital \(mixed\)](#)

[4 Technology for Simulating Power Integrated Systems](#)

[4.1. Introduction](#)

[4.2. Hardware and software design of engine control](#)

[4.3. Proposed design stream: related tools](#)

[4.4. Conclusion](#)

[5 3D Electrothermal Integration](#)

[5.1. Introduction](#)

[5.2. Electrothermal modeling of substrate](#)

[5.3. Heat analysis for 3D ICs](#)

[5.4. Conclusion](#)

[5.5. Heat pipe](#)

[5.6. Conclusion](#)

[6 Substrate Coupling in Smart Power Integration](#)

[6.1. Introduction](#)

[6.2. Part I: smart power integration using the DTI technique](#)

[6.3. Part II: smart power integration using stacked 3D technology](#)

[Conclusion](#)

[C.1. Conclusions](#)

[C.2. Future work](#)

[Appendix: Semiconductor Physical Models](#)

[A.1. Electron and hole densities](#)

[A.2. Intrinsic semiconductors](#)

[A.3. Extrinsic semiconductors](#)

[A.4. Incomplete ionization](#)

[A.5. Mobility](#)

[References](#)

[Index](#)

[End User License Agreement](#)

List of Tables

Chapter 2

[Table 2.1. Advantages and disadvantages of the MOSFET and bipolar transistor](#)

[Table 2.2. Internal bipolar transistor of an IGBT structure](#)

[Table 2.3. Technological changes and consequences on epitaxial IGBT](#)

[Table 2.4. Comparison of the effect of thermal expansion in various modules](#)

Chapter 3

[Table 3.1. The influence of the technological developments of CMOS processes](#)

[Table 3.2. Key technological steps in the CMOS process](#)

[Table 3.3. The influence of the technological developments of voltage and curren...](#)

Chapter 4

[Table 4.1. Design flow and associated tools](#)

Chapter 5

[Table 5.1. Parameters of eight-die model: IC 3D](#)

[Table 5.2. Geometry parameters for the one-via model](#)

[Table 5.3. Properties of the working fluid, copper and porous wick materials use...](#)

Appendix: Semiconductor Physical Models

[Table A.1. Constant parameters used to calculate the amount of incomplete ioniza...](#)

[Table A.2. Constant mobility model: default coefficients for silicon](#)

[Table A.3. Masetti model: default coefficients](#)

[Table A.4. Canali model parameters \(default values for silicon\)](#)

[Table A.5. Default velocity saturation parameters \(for silicon\)](#)

[Table A.6. Default parameters for the doping and temperature-dependent SRH lifet...](#)

[Table A.7. Default coefficients of the Auger recombination model](#)

[Table A.8. Band gap narrowing models: default parameters for silicon](#)

List of Illustrations

Chapter 1

[Figure 1.1. Applications of power devices](#)

[Figure 1.2. System ratings of power devices](#)

[Figure 1.3. V-groove MOSFET structure. For a color version of this figure, see w...](#)

[Figure 1.4. VD-MOSFET structure. For a color version of this figure, see www.ist...](#)

[Figure 1.5. U-MOSFET structure. For a color version of this figure, see www.iste...](#)

[Figure 1.6. LDMOSFET structure. For a color version of this figure, see www.iste...](#)

[Figure 1.7. Dielectric insulation](#)

[Figure 1.8. Standard junction insulation](#)

[Figure 1.9. Passive junction insulation](#)

[Figure 1.10. Active junction insulation](#)

Chapter 2

[Figure 2.1. Generic structure of the IGBT](#)

[Figure 2.2. IGBT equivalent schematic](#)

[Figure 2.3. Simplified equivalent schematic of the IGBT](#)

[Figure 2.4. Decomposition of hole current and electron current](#)

[Figure 2.5. Current lines in normal mode in a half-cell of IGBT \(before reversal...](#)

[Figure 2.6. Current lines after reversal in half a cell of an IGBT, \$J_c \cong 200 \text{ A/cm}^2\$...](#)

[Figure 2.7. Static curve \$J_c = f\(V_{ce}\)\$ with flipped appearance \(Sentaurus simulati...](#)

[Figure 2.8. Appearance of the space charge layer](#)

[Figure 2.9. Different cell forms: a\) square, b\) circular, c\) in continuous tapes...](#)

[Figure 2.10. Tail of current during the opening phase](#)

[Figure 2.11. IGBT with N buffer layer](#)

[Figure 2.12. IGBT with load injection control, referred to as a "homogeneous str...](#)

[Figure 2.13. IGBT with epitaxial structure with buffer layer and reduction in ca...](#)

[Figure 2.14. Comparison of the spread of the space load zone between an IGBT wit...](#)

[Figure 2.15. Static curve \$J_c = f\(V_{ce}\)\$ for a buffer layer with a thickness \$WN = 0...\$](#)

[Figure 2.16. Resistive micro-sounding reading on an IRGPC50S: resistivity and vo...](#)

[Figure 2.17. Static curve \$J_c = f\(V_{ce}\)\$ for the following lifetime in the central ...](#)

[Figure 2.18. Presence of increased conduction zone in epitaxial technology.](#)

[Figure 2.19. Surface view of the cells of an IGBT IRGPC50S, photo taken under an...](#)

[Figure 2.20. Current tail during the opening phase of an IGBT with homogeneous t...](#)

[Figure 2.21. SDB-IGBT technology: Two substrates assembling \(principle\).](#)

[Figure 2.22. Trench technology \(principle\).](#)

[Figure 2.23. Lateral IGBT. For a color version of this figure, see \[www.iste.co.u...\]\(http://www.iste.co.u...\)](#)

[Figure 2.24. Cut and equivalent electrical schematic of the lateral IGBT](#)

[Figure 2.25. DCB power module assembly technology.](#)

[Figure 2.26. Analogy between electrical/thermal resistance](#)

[Figure 2.27. Thermal resistance comparisons](#)

[Figure 2.28. Power module example](#)

[Figure 2.29. Simplified cutting of a power module with possible heat paths](#)

[Figure 2.30. One-dimensional simplified thermal model](#)

[Figure 2.31. Molybdenum and aluminum layer to improve contact between silicon ch...](#)

[Figure 2.32. IGBT static characteristics and temperature coefficient](#)

[Figure 2.33. Mini IPM of Fuji](#)

[Figure 2.34. Internal design of the IPM](#)

[Figure 2.35. Block schematic of the IPM](#)

[Figure 2.36. The IPM in an application](#)

Chapter 3

[Figure 3.1. MOS transistor structure](#)

[Figure 3.2. Current drain voltage characteristics](#)

[Figure 3.3. MOS transistor conduction](#)

[Figure 3.4. Energy band diagram of an MOS structure](#)

[Figure 3.5. Principle of use of CMOS structures in digital circuits](#)

[Figure 3.6. CMOS structure commutation](#)

[Figure 3.7. Aging of NMOS transistors by hot carriers](#)

[Figure 3.8. Cross-sectional view of CMOS](#)

[Figure 3.9. a\) 5V NMOS characteristics. b\) 5V PMOS characteristics. For a color ...](#)

[Figure 3.10. N+ junction characteristics](#)

[Figure 3.11. P+ junction characteristics](#)

[Figure 3.12. Current generated by impact ionization along a silicon bar](#)

[Figure 3.13. The three components of a planar junction](#)

[Figure 3.14. MOS capacitance: I-V characteristics](#)

[Figure 3.15. Influence of the guard ring on the extension of the CEA](#)

[Figure 3.16. Junction protected by a field electrode](#)

[Figure 3.17. Junction protected by a secondary implant](#)

[Figure 3.18. Junction protected by a semiresistive layer](#)

[Figure 3.19. RESURF guardtechnique](#)

[Figure 3.20. Electrical insulation by diffused junctions](#)

[Figure 3.21. Electrical self-insulation by active junction](#)

[Figure 3.22. Electrical insulation by dielectric](#)

[Figure 3.23. Cross-sectional view of a DMOS structure in "up drain" configuratio...](#)

[Figure 3.24. Classical LDMOS transistor configuration](#)

[Figure 3.25. LDMOS RESURF transistor configuration](#)

[Figure 3.26. Self-isolated LDMOS transistor configuration](#)

[Figure 3.27. High-voltage interface \(LV/HV conversion\)](#)

[Figure 3.28. Common source mount](#)

[Figure 3.29. Equivalent diagram in small signals](#)

[Figure 3.30. Gain module](#)

[Figure 3.31. Cascode mount](#)

[Figure 3.32. Small signals equivalent schematic](#)

[Figure 3.33. MOS equivalent schematic](#)

[Figure 3.34. Small signals schematic](#)

[Figure 3.35. Voltage gain: Bode diagram](#)

[Figure 3.36. Gain comparison: with or without “cascode”](#)

[Figure 3.37. Block diagram of the A.O](#)

[Figure 3.38. Differential amplifiers. M5: current source, M1, M2: differential p...](#)

[Figure 3.39. Small signal equivalent differential pair](#)

[Figure 3.40. Common mode differential amplifier](#)

[Figure 3.41. Common mode voltage](#)

[Figure 3.42. \$I_N\$ and \$g_m\$](#)

[Figure 3.43. Nominal low frequency voltage gain, without or with “diode” transis...](#)

[Figure 3.44. \$I_N\$, \$I_p\$, \$I_N+I_P\$](#)

[Figure 3.45. ASIC](#)

[Figure 3.46. Mixed resources: hardware and software](#)

[Figure 3.47. Generic mixed design method](#)

[Figure 3.48. From an idea to IC](#)

Chapter 4

[Figure 4.1. Synoptic of the structure of the engine measure bench. For a color v...](#)

[Figure 4.2. a\) General methodology of mixed design. b\) Our current approach to t...](#)

[Figure 4.3. Simulation results of the two models in MATLAB. For a color version ...](#)

[Figure 4.4. Alta SPW: synoptic](#)

[Figure 4.5. a\) Inverter and b\) block diagram of the three-phase inverter under S...](#)

[Figure 4.6. Co-simulation results. The top three signals are the voltage slots o...](#)

[Figure 4.7. Schematic diagram of a mixed simulation with VHDL-AMS](#)

[Figure 4.8. Simulation of starting a three-phase asynchronous motor described us...](#)

[Figure 4.9. Vectorial or scalar control ASIC architecture](#)

[Figure 4.10. Hardware prototyping board. For a color version of this figure, see...](#)

[Figure 4.11. a\) Distribution of the “hard” and “soft” tasks of the chain. b\) Har...](#)

Chapter 5

[Figure 5.1. a\) Specific depth profile of a 35- \$\mu\text{m}\$ technology \(p+/p- region\); b\) 3...](#)

[Figure 5.2. General steps of 3D-TLE algorithm \(transmission line extractor\)](#)

[Figure 5.3. a\) Voltage map \(layer interfaces: L3/L4\). b\) Corresponding impednce ...](#)

[Figure 5.4. 3D-TLE substrate extractor, e.g. Impedance Z17, capacity and resista...](#)

[Figure 5.5. Model geometry of two TSVs. For a color version of this figure, see ...](#)

[Figure 5.6. Input script description](#)

[Figure 5.7. 3D-TLE extractor setting. For a color version of this figure, see ww...](#)

[Figure 5.8. 2xTSVs model S parameters: a\) S21 magnitude without de-embedding; b\)...](#)

[Figure 5.9. S parameters study for the 2xTSVs \(ADS\) model](#)

[Figure 5.10. Comparison of S12 between 2TSV with and without SUB model: measurem...](#)

[Figure 5.11. S21 collision/distribution/scattering parameters. For a color versi...](#)

[Figure 5.12. Spreading impedance of the temperature](#)

[Figure 5.13. a\) Temperature command profile; simulation date: 2.2 \$\mu\$ s. b\) Tempera...](#)

[Figure 5.14. Diagram of the optical lithography tool step by step and repeated. ...](#)

[Figure 5.15. Comparison of lithography wavelength trends with characteristic siz...](#)

[Figure 5.16. a\) A planar IC; b\) a 3D IC with two dies; c\) a 3D IC with five dies](#)

[Figure 5.17. Typical baseline processor](#)

[Figure 5.18. Temperatures of functional blocks on planar and 3D ICs. For a color...](#)

[Figure 5.19. Typical finite element mesh: elements, nodes and edges](#)

[Figure 5.20. A simple thermal model for 3D IC chip](#)

[Figure 5.21. a\) Schematic of IC 3D structure \(without vias\); b\) heat transfer mo...](#)

[Figure 5.22. a\) Schematic of 3D IC structure with TSVs. b\) Heat transfer model](#)

[Figure 5.23. Different layer numbers influence on the 3D IC top layer temperatur...](#)

[Figure 5.24. Surface ratio \$r\$ and dies' numbers influence on the 3D IC top layer ...](#)

[Figure 5.25. Temperature change with surface ratio \$r\$ \(\$n = 8\$ \).](#)

[Figure 5.26. 3D thermal simulation work flow. For a color version of this figure...](#)

[Figure 5.27. a\) Bottom and b\) top layer temperature distribution of four TSVs wi...](#)

[Figure 5.28. Ground and power networks structures. For a color version of this f...](#)

[Figure 5.29. Electrical dynamical element cell](#)

[Figure 5.30. 3xRLC series model SPICE script](#)

[Figure 5.31. "three-segment RLC" compact model](#)

[Figure 5.32. a\) Input voltage source; \(b\) output comparison between MNA and ADS,...](#)

[Figure 5.33. Dynamic thermal elementary cell](#)

[Figure 5.34. Pulse signal definition](#)

[Figure 5.35. 3D IC electrothermal coupling flow](#)

[Figure 5.36. a\) Electrical compact mode; b\) 2D geometry; and c\) thermal compact ...](#)

[Figure 5.37. S parameters of the ADS model 1-TSV \(valid for the frequency below ...](#)

[Figure 5.38. Signal transient integrity analysis for the 1-TSV 2.5 GHz model. a\)...](#)

[Figure 5.39. S parameters with a\) error curve and b\) maximum temperature curve f...](#)

[Figure 5.40. a\) Electrical compact mode, b\) 2D geometry and c\) compact thermal m...](#)

[Figure 5.41. S parameters with a\) error curve and b\) maximum temperature curve f...](#)

[Figure 5.42. S parameters with a\) error curve and b\) maximum temperature curve f...](#)

[Figure 5.43. Schematic of approximate network of thermal resistance of FHP. For ...](#)

[Figure 5.44. Contour map of the resistance ratio RHP RHS plotted as a function o...](#)

[Figure 5.45. Flat heat pipe with different heating/cooling configurations: a\) co...](#)

[Figure 5.46. Temperature profile: a\) comparison between COMSOL and pub with 50 W...](#)

[Figure 5.47. Comparison of the velocities at the center of the vapor chamber: a\)...](#)

[Figure 5.48. Perssure \(Maylab calculatios\) at the wick-vapor interface: a\) compa...](#)

Chapter 6

[Figure 6.1. The deep trench isolation structure](#)

[Figure 6.2. The structure of cLDMOS with deep trench isolation](#)

[Figure 6.3. The drain and bulk currents for a\) nLDMOS and b\) pLDMOS, without tre...](#)

[Figure 6.4. a\) Potential distribution and b\) electric field distribution in nLDM...](#)

[Figure 6.5. a\) Potential distribution and b\) electric field distribution in pLDM...](#)

[Figure 6.6. The drain currents of a\) nLDMOS and b\) pLDMOS, at \$|V_{GS}| = 3\text{ V}\$, with...](#)

[Figure 6.7. Simplified cross-section, showing the cLDMOS, the CMOS and the paras...](#)

[Figure 6.8. The injection collected ratio of a\) pLDMOS and b\) pMOS in two cases ...](#)

[Figure 6.9. The potential contour distributions in the case of a\) without P+ and...](#)

[Figure 6.10. Substrate noise injection mechanisms in a digital inverter](#)

[Figure 6.11. The 2D structure of the nMOS with DTI](#)

[Figure 6.12. The potential distribution of the nMOS structure with DTI](#)

[Figure 6.13. a\) The saturation drain current and b\) the bulk electrode current d...](#)

[Figure 6.14. a\) The saturation drain current and b\) the bulk current, as a funct...](#)

[Figure 6.15. a\) The saturation drain current and b\) the bulk current, as a funct...](#)

[Figure 6.16. The 2D structure of the pMOS with DTI](#)

[Figure 6.17. The potential distribution of the pMOS structure with DTI](#)

[Figure 6.18. a\) The saturation drain current, b\) the bulk electrode current and ...](#)

[Figure 6.19. a\) The saturation drain current, b\) the bulk electrode current and ...](#)

[Figure 6.20. a\) The saturation drain current, b\) the bulk electrode current and ...](#)

[Figure 6.21. The 2D structure of the CMOS with DTI](#)

[Figure 6.22. The potential distribution in the CMOS structure with DTI](#)

[Figure 6.23. The temperature waveform in the CMOS structure with DTI](#)

[Figure 6.24. The potential distribution in the CMOS structure with DTI when the ...](#)

[Figure 6.25. a\) The potential distribution and b\) the voltages and output-current...](#)

[Figure 6.26. The potential distribution in the CMOS structure with DTI when the ...](#)

[Figure 6.27. a\) The potential distribution and b\) the voltages and output-current...](#)

[Figure 6.28. The cost and performance comparison between the various technologie...](#)

[Figure 6.29. An example of a heterogeneous 3D system-on-chip](#)

[Figure 6.30. TSV- and RDL-based 3D integration](#)

[Figure 6.31. The 2D structure of the thinned stratum with nMOS](#)

[Figure 6.32. Potential distribution for RDL floating for \$TSUB = 10 \mu m\$ and TOXTSV...](#)

[Figure 6.33. a\) The saturation drain current and b\) the bulk electrode current d...](#)

[Figure 6.34. The saturation drain current as a function of the substrate thickne...](#)

[Figure 6.35. The bulk current as a function of the substrate thickness for diffe...](#)

[Figure 6.36. a\) The drain current and b\) the bulk current as a function of the T...](#)

[Figure 6.37. Potential distribution for TSV floating for \$TSUB = 10 \mu m\$, \$TOXTSV = ...\$](#)

[Figure 6.38. Potential distribution for \$TSUB = 10 \mu m\$ and \$TOXTSV = 0.05 \mu m\$](#)

[Figure 6.39. a\) The saturation drain current and b\) the bulk electrode current d...](#)

[Figure 6.40. The 2D structure of the thinned stratum with pMOS](#)

[Figure 6.41. Potential distribution for RDL floating for \$TSUB = 10 \mu m\$ and \$TOXTSV...\$](#)

[Figure 6.42. a\) The saturation drain current, b\) the bulk electrode current and ...](#)

[Figure 6.43. The saturation drain current as a function of the TSV spacing at va...](#)

[Figure 6.44. The bulk voltage as a function of the TSV spacing for different TSV...](#)

[Figure 6.45. The bulk current as a function of the TSV spacing for different TSV...](#)

[Figure 6.46. The saturation drain current as a function of the substrate thickne...](#)

[Figure 6.47. The bulk current as a function of the substrate thickness at variou...](#)

[Figure 6.48. The bulk voltage as a function of the substrate thickness at variou...](#)

[Figure 6.49. Potential distribution for TSV floating for \$TSUB = 10 \mu m\$, \$TOXTSV = ...\$](#)

[Figure 6.50. Body-voltage for RDL 0.5 \$\mu\text{m}\$ ON case
TSUB = 5 \$\mu\text{m}\$](#)

[Figure 6.51. Potential distribution for TSUB = 10
 \$\mu\text{m}\$ and TOXTSV = 0.05 \$\mu\text{m}\$](#)

[Figure 6.52. a\) The saturation drain current, b\) the
bulk electrode current and ...](#)

[Figure 6.53. The CMOS sensitive regions](#)

[Figure 6.54. The CMOS potential distribution for a\)
floating RDL and b\) floating...](#)

[Figure 6.55. The 2D structure of TSV-CMOS with
floating nMOS bulk contact](#)

[Figure 6.56. a\) The potential distribution and b\) the
voltages and output curren...](#)

[Figure 6.57. The structure of TSV-CMOS with
floating nMOS bulk contact](#)

[Figure 6.58. a\) The potential distribution and b\) the
voltages and output-curren...](#)

[Figure 6.59. The structure of TSV-CMOS with
floating pMOS bulk contact](#)

[Figure 6.60. a\) The potential distribution and b\) the
voltages and output curren...](#)

[Figure 6.61. The structure of TSV-CMOS with
floating pMOS bulk contact and with ...](#)

[Figure 6.62. a\) The potential distribution and b\) the
voltages and output curren...](#)

[Figure 6.63. 3D cross-section of TSV-CMOS mixed-
mode coupling](#)

[Figure 6.64. a\) Y-cut potential distribution and b\)
the voltages and output curr...](#)

[Figure 6.65. System via and striplines: a\) 3D-structure and b\) cut along the X-a...](#)

[Figure 6.66. Electric field map, transient regime](#)

[Figure 6.67. Voltage at different probe points: excitation: pulse on Port0 \(see ...](#)

[Figure 6.68. Transmission parameters: S12 and S21](#)

[Figure 6.69. System via and striplines bended at 90°](#)

[Figure 6.70. Voltage at different probe points: excitation: pulse on Port0 \(see ...](#)

Appendix: Semiconductor Physical Models

[Figure A.1. Dependence of ionization fraction on total doping for a\) phosphorus ...](#)

[Figure A.2. The energy of the dopant band peak \$E_{\text{dop}}\$ and the activation energy of...](#)

[Figure A.3. Comparison of ionization fractions for three models at \$T = 300 \text{ K}\$](#)

[Figure A.4. The fraction between measured conductivity mobility and Hall mobilit...](#)

[Figure A.5. Comparison between our modified model and Altermatt et al.'s model f...](#)

[Figure A.6. Dependence of constant mobility on temperature](#)

[Figure A.7. Doping dependent mobility at \$T = 300 \text{ K}\$](#)

[Figure A.8. Masetti model: doping-dependent mobility at \$T = 300 \text{ K}\$](#)

[Figure A.9. Temperature dependence of the electron drift velocity according to t...](#)

[Figure A.10. The three recombination mechanisms determining recombination lifeti...](#)

[Figure A.11. Doping dependence of the SRH lifetimes](#)

[Figure A.12. Effective lifetime dependence on carrier concentration](#)

[Figure A.13. The indirect gap in Si, showing the difference between the rigid an...](#)

[Figure A.14. Comparison of electrical BGN models](#)

Smart Power Integration

Mohamed Abouelatta

Ahmed Shaker

Christian Gontrand

ISTE

WILEY

First published 2022 in Great Britain and the United States by ISTE Ltd and John Wiley & Sons, Inc.

Apart from any fair dealing for the purposes of research or private study, or criticism or review, as permitted under the Copyright, Designs and Patents Act 1988, this publication may only be reproduced, stored or transmitted, in any form or by any means, with the prior permission in writing of the publishers, or in the case of reprographic reproduction in accordance with the terms and licenses issued by the CLA. Enquiries concerning reproduction outside these terms should be sent to the publishers at the undermentioned address:

ISTE Ltd

27-37 St George's Road

London SW19 4EU

UK

John Wiley & Sons, Inc.

111 River Street

Hoboken, NJ 07030

USA

www.iste.co.uk

www.wiley.com

© ISTE Ltd 2022

The rights of Mohamed Abouelatta, Ahmed Shaker and Christian Gontrand to be identified as the authors of this work have been asserted by them in accordance with the Copyright, Designs and Patents Act 1988.

Any opinions, findings, and conclusions or recommendations expressed in this material are those of the author(s), contributor(s) or editor(s) and do not necessarily reflect the views of ISTE Group.

Library of Congress Control Number: 2022939122

British Library Cataloguing-in-Publication Data

A CIP record for this book is available from the British Library

ISBN 978-1-78630-837-5

Preface

Smart integration is a process in which an existing system infrastructure is upgraded through the integration of multiple technologies, for example, automated sensors, advanced automated controls and forecasting systems. A smart grid allows for interaction between the consumers and enables optimal use of energy and communication systems based on price preferences and system technical stresses, without forgetting the environmental aspect.

The continuous reduction in dimensions and the need for increasingly high power density have highlighted the need for ever more efficient structures. Smart power technology has been developed to meet this demand. This technology makes specific use of (L)DMOS devices, offering new solutions because of its unique high voltage and high current characteristics. The operation of these devices is accompanied by a number of phenomena. Good modeling makes it possible to account for these phenomena and predict the physical behavior of the transistor prior to production. To this, we add an axis that has become unavoidable: the entanglement between devices, circuits, connections and substrates.

(Micro)grid designs have evolved significantly in recent years with the incorporation of information and communication technology (ICT) solutions, such as artificial intelligence (AI) and machine learning (ML). A smart microgrid, equipped with sensors and automation controls, can efficiently perform load profiling and forecasting, generation management, load prioritization, etc. A go-to example is the vehicles that are quickly becoming a center of communication, navigation and connectivity. Automotive solutions will integrate with smart city infrastructures,

personal devices and in-vehicle services to become part of a connected whole.

This book introduces different domains and tools and allows the reader to develop their understanding of smart power systems through real studies. Knowledge of high school mathematics is sufficient to progress through these studies.

Mohamed Abdelhamid Abouelatta
Ahmed Shaker Ahmed Zaki Ghazala
Christian Gontrand
January 2021

1

Overview of Smart Power Integration

1.1. Introduction

Since 1965, integrated circuit (IC) technology has followed Moore's law which states that the number of integrated devices doubles every 18 months. This growth is partly due to an increase in the size of ICs that can be produced. However, the dominant effect is due to the reduction in feature size of component devices that are integrated. The reduction of feature size tends to bring advantages of increased speed and the possibility to operate at lower voltages, allowing reduced power consumption. These advantages make technology shrinkage very attractive for technical performance reasons, as well as cost.

However, there are many applications where voltage cannot be reduced for external reasons. There are three areas where this is the case: power electronics, automotive applications and wide dynamic range circuits. In such applications, system integration of high voltage, analog and digital circuitry on a single IC is attractive in order to gain advantage in terms of miniaturization, reliability, efficiency and cost. However, in order to make these gains, the conflict of reducing voltage due to technology feature size has to be resolved with the requirements for operation at continued relatively high voltage.

The different operation and interface requirements of high voltage, analog and digital require a technology development optimized for these system requirements. Different technologies have been developed to address

these applications, such as smart power and various bipolar-CMOS-DMOS (BCD) processes.

Smart power integrated circuits (PICs) that monolithically integrate low-loss power devices and control circuitry have attracted much attention across a wide range of applications. These ICs improve system reliability, reduce volume and weight and increase overall efficiency.

Considerable effort has been put into the development of smart power devices for automotive electronics, peripheral computer appliances and portable equipment, such as cell phones, video cameras, and so on.

Commonly used smart power devices are the lateral double diffused MOS Field Effect Transistor (LDMOSFETs) and lateral insulated gate bipolar transistors (LIGBTs) implemented in bulk silicon or silicon on insulator (SOI). The main challenges in the development of these devices are obtaining the best trade-off between specific ON-resistance $R_{ON,SP}$ ($R_{ON} \times \text{area}$) and breakdown voltage (BV), and shrinking feature size without degrading device characteristics.

1.2. Smart PIC applications

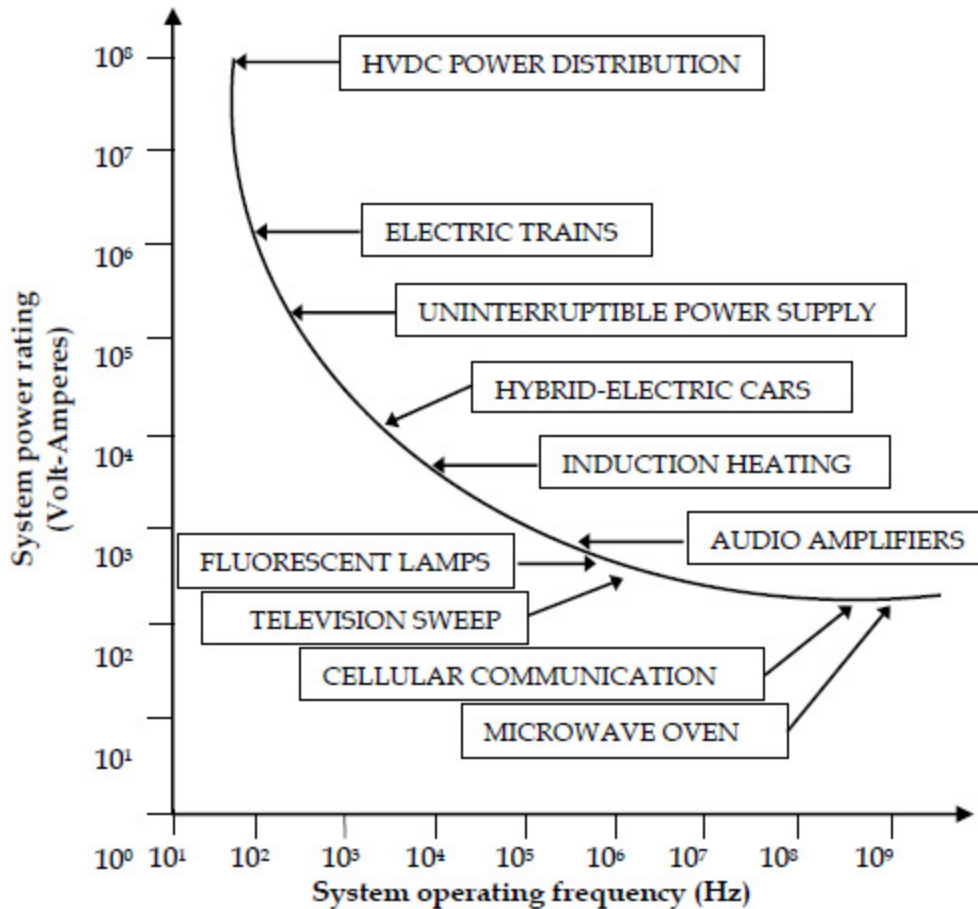


Figure 1.1. *Applications of power devices*

Smart PIC technology is expected to have an impact in all areas in which discrete power semiconductor devices are currently being used. It is anticipated that this technology will open up new applications based upon the added features of smart controls. In [Figure 1.1](#), applications of power devices are shown as a function of operating frequency. Another classification approach of these applications involves current and voltage handling requirements, as shown in [Figure 1.2](#). Some of these applications are listed in the following subsections.

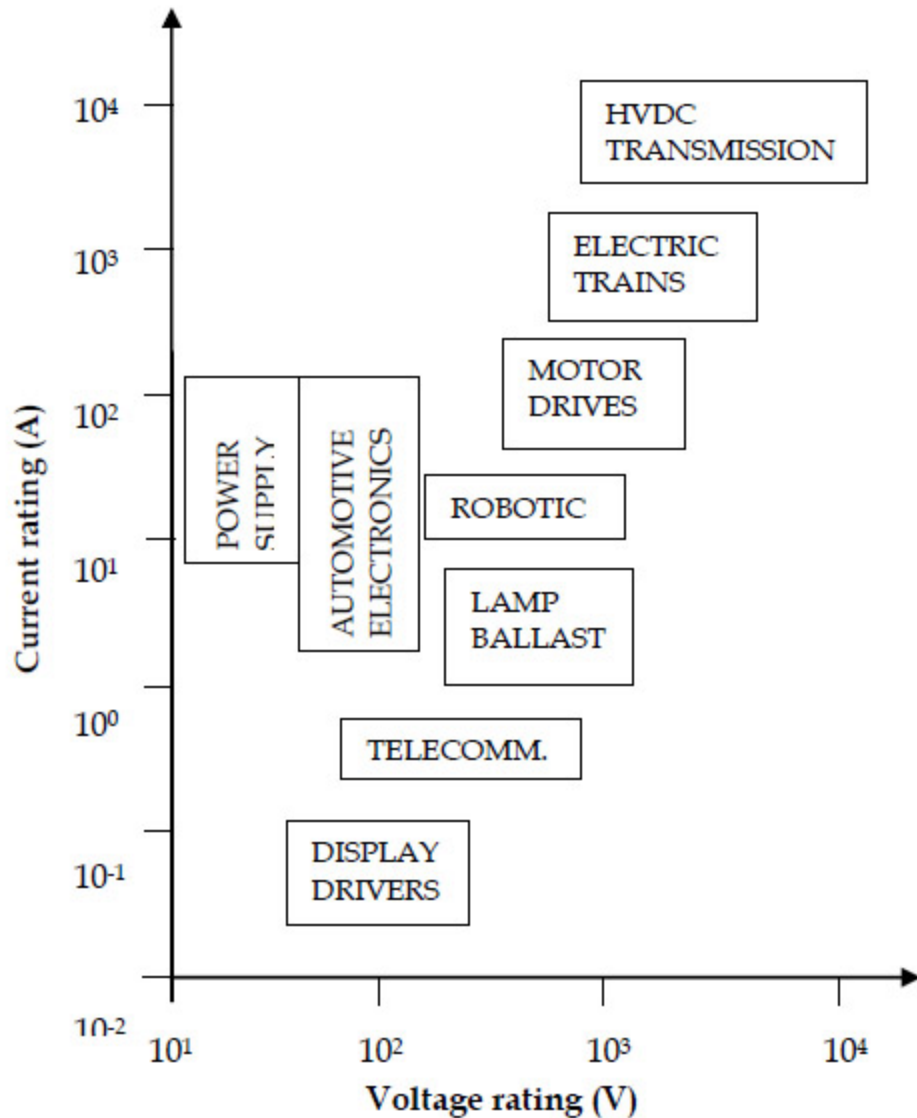


Figure 1.2. *System ratings of power devices*

1.2.1. Flat panel displays

The popularity of portable electronic products such as cell phones and notebook computers has generated significant demand for flat panel displays. These displays are usually liquid crystal displays (LCD) or electro-luminescence (EL) panels arranged in a matrix with large number of column and row drivers (e.g. 640 × 480 for VGA resolution).

Although the required voltage may be high, the current level is low (usually in the mA range). Smart PICs with as

many as 80 output channels have been fabricated on a monolithic chip.

1.2.2. Computer power supplies and disk drivers

Computer systems are developing continuously in terms of speed and processing capabilities. This is made possible by using higher density Very Large-Scale Integration (VLSI) technology. However, the increased power requirement has resulted in an increase in the physical size of the power supply. In 1976, the CPU board and power supply each represented one-third of the total physical volume of a computer system. By the 1990s, the power supply had grown to 50% of the physical volume while the CPU board had shrunk to about 20%. To reverse this trend, it is necessary to develop smart PIC technology to improve the density and hence the volume of the power supplies.

1.2.3. Variable speed motor drives

Variable-speed motor drives are being developed to reduce power loss in all applications. The improvement in performance requires smart power technology that can operate at relatively high frequencies with low power losses. This translates to a low ON-state voltage drop at high current levels, fast switching speed and rugged operation. For smart PIC implementation, additional consideration, such as level shifting to and from high voltages, over-temperature, over-current, over-voltage and short-circuit protection are more critical.

1.2.4. Factory automation

Advanced numerical control and robotic systems require efficient smart PIC technology to create a distributed power control network under the management of a central

computer. The smart PICs for this application must be capable of providing AC or DC power to various loads, such as motors, solenoids, arc welders, and so on. They are also required to perform diagnostic, protection and feedback functions.

1.2.5. Telecommunications

One of the high-volume markets for smart power technology is in telecommunications. The technology required for these applications must be capable of integrating multiple high-voltage, high-current devices on a single chip. At present, this has been achieved using MOS devices fabricated using dielectric insulation. Improvements are required to reduce the cost of the dielectric insulation fabrication process. Ongoing development on direct wafer bonding has been promising in terms of providing a cost-effective process.

1.2.6. Appliance controls

The main benefit of using smart PICs in appliance control is to provide improvements in performance and efficiency. Onboard sensors can also provide more precise controls (e.g. temperature settings). Simple domestic appliances, such as toasters, washing machines and irons, are appearing with smart PICs for this reason.

1.2.7. Consumer electronics

Smart PICs are required for a large variety of entertainment systems such as CD players, tape recorders, VCRs, etc. For example, a monolithic motor control IC that regulates the speed of the motor, while minimizing power losses, is essential to all battery-operated consumer entertainment systems. Development of improved lateral